REGULAR PAPER

Analysis of energy states of two-dimensional electron gas in pseudomorphically strained InSb high-electron-mobility transistors taking into account the nonparabolicity of the conduction band

To cite this article: Yui Nishio *et al* 2016 *Jpn. J. Appl. Phys.* **55** 084301

Japanese Journal of Applied Physics **55**, 084301 (2016)
http://doi.org/10.7567/JJAP.55.084301

REGULAR PAPER

Analysis of energy states of two-dimensional electron gas in pseudomorphically strained InSb high-electron-mobility transistors taking into account the nonparabolicity of the conduction band

Yui Nishio*, Takato Sato, Naomi Hirayama, Tsutomu Iida, and Yoshifumi Takanashi

Department of Materials Science and Technology, Faculty of Industrial Science and Technology, Tokyo University of Science, Katsushika, Tokyo 125-8585, Japan

*E-mail: 8213703@alumni.tus.ac.jp

Received December 2, 2015; accepted May 10, 2016; published online July 13, 2016

We propose a high electron mobility transistor with a pseudomorphically strained InSb channel (InSb-PHEMT) having an InSb composite channel layer in which the $Al_yIn_{1-y}Sb$ sub-channel layer is inserted between the InSb channel and the $Al_xIn_{1-x}Sb$ barrier layers to increase the conduction-band offset (ΔE_C) at the heterointerface between the InSb channel and the $Al_xIn_{1-x}Sb$ barrier layers. The energy states for the proposed InSb-PHEMTs are calculated using our analytical method, taking account of the nonparabolicity of the conduction band. For the proposed InSb-PHEMTs, putting the sub-channel layers into the channel is found to be effective for obtaining a sufficiently large ΔE_C (~0.563 eV) to restrain electrons in the channel and increase the sheet concentration of two-dimensional electron gas to as high as $2.5 \times 10^{12}\,cm^{-2}$, which is comparable to that of InAs-PHEMTs. This also leads to a large transconductance of PHEMTs. In the proposed InSb-PHEMTs, electrons are strongly bound to the channel layer compared with InAs-PHEMTs, despite the effective mass at the conduction band ($0.0139\,m_0$) of InSb being smaller than that of InAs and ΔE_C for the InSb-PHEMTs being 25% smaller than that for the InAs-PHEMTs. This is because the bandgap energy of InSb is about one-half that of InAs, and hence, the nonparabolicity parameter of InSb is about twice as large as that of InAs.

1. Introduction

Recently, high-electron-mobility transistors (HEMTs) with a pseudomorphically strained InAs channel (InAs-PHEMTs) have received much attention because of their high-speed operation and their applicability to high-speed ICs.[1–4] They have exhibited a current-gain cutoff frequency f_T of 710 GHz, a maximum oscillation frequency f_{max} of 1.5 THz, and a transconductance G_m of 2.114 S/mm.[1,2] Among the binary III–V semiconductors, InSb has the highest electron mobility, and hence, InSb-PHEMTs are expected to exhibit even higher performance than conventional $In_{0.53}Ga_{0.47}As$-HEMTs and InAs-PHEMTs. PHEMTs with pseudomorphically strained InSb as the channel material have been developed so far.[5,6] They exhibited f_T of 305 GHz, f_{max} of 500 GHz, and G_m of 1.1 S/mm.[5,6]

According to a simple model, the subband energy is well known to be inversely proportional to the effective mass of electrons m_c^* at the bottom of the conduction band.[7] The m_c^* of InSb is $0.013\,m_0$ and is the smallest among III–V compound semiconductors.[8] Using this m_c^* value causes the subband energies of InSb-PHEMTs to be much higher than those for $In_{0.53}Ga_{0.47}As$-HEMTs and InAs-PHEMTs. As a result, the threshold voltage V_{TH} of InSb-PHEMTs may shift toward the normally-off side because the Fermi energy E_F must be located above the subband energies to generate the two-dimensional electron gas (2DEG) in the channel. This is the first issue for InSb-PHEMTs. Next, the density of states for InSb becomes much lower than those for $In_{0.53}Ga_{0.47}As$-HEMTs and InAs-PHEMTs as a result of the lower effective mass of InSb, leading to the fact that the sheet electron concentration n_s of InSb-PHEMTs may be much lower than those of $In_{0.53}Ga_{0.47}As$-HEMTs and InAs-PHEMTs, despite their high electron mobility of $80{,}000\,cm^2\,V^{-1}\,s^{-1}$ in nature.[9] This may give rise to a lower transconductance of InSb-PHEMTs compared with those of $In_{0.53}Ga_{0.47}As$-HEMTs and InAs-PHEMTs. This is the second issue for InSb-PHEMTs.

The InSb-PHEMTs recently reported have a relatively thick channel layer (15–20 nm in thickness) and a lower conduction-band offset ΔE_C of 0.11 eV between the $Al_xIn_{1-x}Sb$ barrier and the InSb channel layers.[5,6] In this layer structure, the energy states of electrons in the channel are close to that of bulk InSb, and hence the merits, such as higher n_s and G_m accompanying the adoption of the quantum-well structure in the channel cannot be sufficiently brought out.

According to Kane,[10,11] for InSb with an unstrained energy gap E_g as small as 0.175 eV at room temperature,[12] the nonparabolicity of the conduction band must be taken into account. Recently, we have pointed out that the nonparabolicity of the conduction band should be taken into account even for InAs-PHEMTs in which the InAs with a small E_g of 0.36 eV is used as the channel.[13,14] In this model, we have defined an energy-dependent effective mass to calculate the energy states of 2DEG in the InAs channel of PHEMTs by using a standard perturbation theory and solving both the Schrödinger and Poisson equations self-consistently.[13,14] We have also applied this analytical method to InAs-PHEMTs and have succeeded in explaining their characteristics.[15] The threshold voltage V_{TH} calculated using the nonparabolic energy band agreed well with that obtained experimentally, while V_{TH} calculated using the parabolic energy band was about 0.2 V larger than that calculated using the nonparabolic energy band.

In this study, we have applied our theory[13–15] to InSb-PHEMTs for determining not only V_{TH} but n_s of InSb-PHEMTs in which the nonparabolicity of the conduction band for the strained InSb channel layer is very strong.[10] In Sect. 2, the device structure employed in the calculation is described in detail, and the analytical method used in this work is outlined in Sect. 3. In particular, an InSb-PHEMT with a composite channel is proposed to simultaneously solve the issues concerning not only V_{TH} but n_s for InSb-PHEMTs. In Sect. 4, we emphasize the importance of taking into account the nonparabolicity of the conduction band in InSb-PHEMTs by comparing the results calculated using

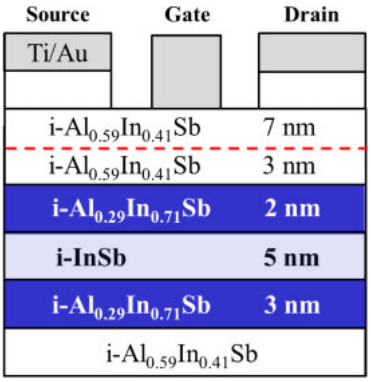

Fig. 1. (Color online) Schematic cross sections of pseudomorphically strained HEMT with $Al_{0.59}In_{0.41}Sb/InSb/Al_{0.59}In_{0.41}Sb$ composite channel layer. The dashed line represents the δ-doped layer.

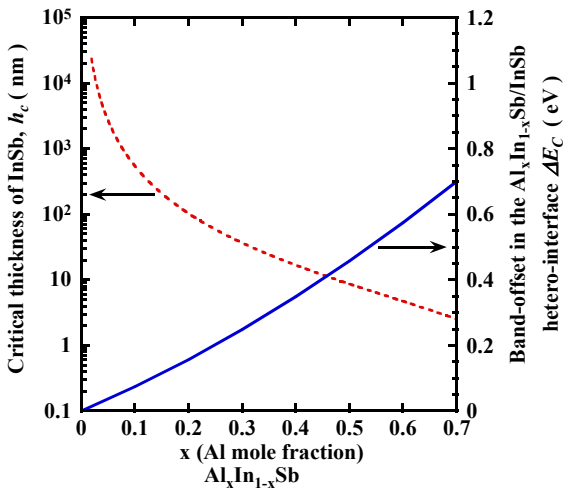

Fig. 2. (Color online) Critical thickness of InSb and conduction-band offset ΔE_C at $Al_xIn_{1-x}Sb/InSb$ heterointerface. The former was estimated using the theory by Matthews and co-workers[16,17] and People and Bean,[18] and the latter the theory by Krijn.[19]

the nonparabolic and parabolic energy bands. In Sect. 5, conclusions are drawn.

2. Device structure

In the previously reported InSb-PHEMTs with strained InSb as the channel layer and $Al_{0.15}In_{0.85}Sb$ as the barrier layer,[5,6] a high concentration of electrons is not expected. This is because the conduction-band offset ΔE_C at the $Al_{0.15}In_{0.85}Sb/InSb$ heterointerface is restricted to as low as 0.11 eV.

Figure 1 shows the schematic cross section of the InSb-PHEMT with a composite channel that we propose in this paper. In this PHEMT, we can substantially increase the ΔE_C at the $Al_xIn_{1-x}Sb/InSb$ heterointerface because the Al mole fraction of the $Al_xIn_{1-x}Sb$ barrier layer can be increased by putting the $Al_yIn_{1-y}Sb$ sub-channel layer between the $Al_xIn_{1-x}Sb$ barrier and the InSb channel layers. The epitaxial layers in the proposed PHEMT are an $Al_{0.59}In_{0.41}Sb$ layer, a composite channel, an $Al_{0.59}In_{0.41}Sb$ spacer layer (3 nm), a Si δ-doping layer, and an $Al_{0.59}In_{0.41}Sb$ barrier layer (7 nm). The composite channel consists of a lower $Al_{0.29}In_{0.71}Sb$ sub-channel (3 nm), an undoped InSb channel layer (5 nm), and an upper $Al_{0.29}In_{0.71}Sb$ sub-channel (2 nm). The thickness of the InSb layer in the $Al_xIn_{1-x}Sb/InSb$ lattice-mismatched material system must be within the critical thickness h_C. The theory for h_C was derived by Matthews and co-workers[16,17] and People and Bean,[18] the former being based on the mechanical equilibrium model and the latter based on the energy-balance model. The h_C of the InSb layer in the composite channel was calculated using the theory derived by People and Bean[18] and then, the thickness of the InSb channel layer was set to be 5 nm. In this calculation, the crystal distortion due to a lattice mismatch between the $Al_xIn_{1-x}Sb$ barrier layer and the substrate, e.g., GaAs, is assumed to be relaxed. The conduction-band offset ΔE_C at the $Al_xIn_{1-x}Sb/InSb$ heterointerface and E_g of InSb were estimated using the well-known Krijn's interpolation equation.[19–23] The results of h_C for the InSb layer in the composite channel and ΔE_C at the $Al_xIn_{1-x}Sb/InSb$ heterointerface corresponding to h_C are shown in Fig. 2. In addition, the material parameters required for this calculation are summarized in Tables I[24–28] and II.[19–23] Since the lattice-constants of InSb channel and sub-channel layers are the same as that of the buffer layer after these layers have been grown on the buffer layer, the respective strain of these layers is specified by the difference in the lattice-constants of each layer and the buffer layer.[16] The effective conduction-band offset $\Delta E_{C,eff}$ for the proposed InSb-PHEMTs was 0.563 eV, which is about 25% smaller than that for InAs-PHEMTs (0.74 eV).[15] As a matter of course, the thickness of sub-channel layers is set to be less than their critical thickness. Here, $\Delta E_{C,eff}$ is defined as the sum of ΔE_C at the $Al_{0.59}In_{0.41}Sb/Al_{0.29}In_{0.71}Sb$ heterointerface and that at the $Al_{0.29}In_{0.71}Sb/InSb$ heterointerface.[15]

Table I. Conduction-band offset used in the calculation of quantum states for InSb-PHEMTs.[26–30]

Heterostructure	ΔE_C (eV)
$Al_{0.59}In_{0.41}Sb/Al_{0.29}In_{0.71}Sb$	0.280
$Al_{0.29}In_{0.71}Sb/InSb$	0.283
$Al_{0.59}In_{0.41}Sb/InSb$	0.563

Table II. Material parameters used in the calculation of quantum states for InSb-PHEMTs.[21–25]

Material	m_c^*/m_0	$\varepsilon_s/\varepsilon_0$	E_g (eV)
$Al_{0.59}In_{0.41}Sb$	0.0523	13.6	1.28
$Al_{0.29}In_{0.71}Sb$	0.0328	15.3	0.72
InSb	0.0139	17.0	0.22

3. Analytical method

Our analytical method is described in detail elsewhere.[13,14] Briefly, the nonparabolicity is taken into account by defining an energy-dependent effective mass based on the $\mathbf{k}\cdot\mathbf{p}$ perturbation theory:[10]

$$m^*(z,E) = m_c^*(z)\{1+\alpha(z)[E-E_C(z)]\}, \quad (1)$$

where z is the distance from the surface, $m_c^*(z)$ is the effective mass at the bottom of the conduction band, and $E_C(z)$ is the conduction-band energy. In addition, α is a nonparabolicity parameter equal to $1/E_g$, E_g being the bandgap energy of the InSb channel.

As a result, the Schrödinger and Poisson equations to be solved are expressed as

$$\left(-\frac{\hbar^2}{2m_c^*(z)\{1+\alpha(z)[E_{n\mathbf{k}}-E_C(z)]\}}\frac{\partial^2}{\partial z^2}+E_C(z)+\frac{\hbar^2k^2}{2m_c^*(z)\{1+\alpha(z)[E_{n\mathbf{k}}-E_C(z)]\}}\right)\psi_{n\mathbf{k}}(z)=E_{n\mathbf{k}}\psi_{n\mathbf{k}}(z), \quad (2)$$

$$\frac{d}{dz}\left[\varepsilon(z)\frac{d}{dz}\varphi(z)\right]=-e[N_D^+(z)-n(z)], \quad (3)$$

where $E_{n\mathbf{k}}$ is the eigenvalue energy, $\psi_{n\mathbf{k}}(z)$ the eigenfunction, $\varphi(z)$ the static potential, $\varepsilon(z)$ the dielectric constant, $N_D^+(z)$ the ionized donor density, and $n(z)$ the electron density. The Schrödinger equation was solved using a standard perturbation theory approach.[7] That is, we regarded the terms including α as the perturbed Hamiltonian [Eq. (5)] and regarded the rest of the terms as the unperturbed Hamiltonian [Eq. (4)]:

$$H_0=-\frac{\hbar^2}{2}\frac{\partial}{\partial z}\left[\frac{1}{m_c^*(z)}\frac{\partial}{\partial z}\right]+E_C(z), \quad (4)$$

$$H'=\frac{\hbar^2k^2}{2m_c^*(z)}-\alpha(z)[E_{n\mathbf{k}}-E_C(z)]^2. \quad (5)$$

The Schrödinger equation for the unperturbed Hamiltonian is written as

$$H_0\xi_n(z)=E_n^0\xi_n(z), \quad (6)$$

where E_n^0 and $\xi_n(z)$ correspond to the eigenvalue and the eigenequation, respectively. The electron density in the channel is given by calculating

$$n(z)=\sum_n\int_{E_n}^{\infty}\frac{\rho_n(E)}{1+\exp[(E-E_F)/kT]}|\psi_{n\mathbf{k}}(z)|^2\,dE, \quad (7)$$

where $\rho_n(E)$ is the density of states and E_F is the Fermi energy.

In our theory, the exchange–correlation energy is also taken into account.[29] The calculation is by the finite difference method.[30] First the Poisson equation [Eq. (3)] is solved to yield the potential profile. Under this potential profile, the Schrödinger equation [Eq. (2)] is solved using the perturbation theory to yield $E_{n\mathbf{k}}$ and $\psi_{n\mathbf{k}}(z)$. Then Eq. (7) is used to determine the new concentration profile of electrons. This calculation process is continued until the electrostatic potential converges to within an error of the order of 10^{-4} eV over the whole range. The subband energy E_n is obtained by taking the extreme limit of $\mathbf{k}\to 0$ for $E_{n\mathbf{k}}$.

In InAs-PHEMTs, it was shown that for each subband energy, the value obtained from the second-order perturbation was less than one-tenth that obtained from the first-order perturbation, and hence it is sufficient to simply take into account the first-order perturbation in the calculation process.[14] In addition, most of electrons were found to occupy the first subband. Therefore, we need only consider the first subband within an approximation to the first-order perturbation in order to estimate the energy state of 2DEG in InAs-PHEMTs. On the contrary, the effective mass parameter α of InSb is about two times that of InAs because the E_g of InSb in PHEMTs is as small as 0.22 eV and is about half that of InAs. Note that the E_g of strained InSb is slightly larger than that of unstrained InSb because the InSb channel layer in PHEMTs has a strain due to a mismatch between the InSb channel and the $Al_xIn_{1-x}Sb$ barrier layers, as described in Sect. 3. Therefore, the perturbation theory does not hold for a subband of higher than the second order because the difference between the subband energy E_n and the conduction-band energy E_C may exceed the E_g of InSb [Eq. (5)]. Then, in this theory, only the first subband was taken into account within an approximation to the first-order perturbation, assuming that most electrons occupy the first subband as in InAs-PHEMTs.

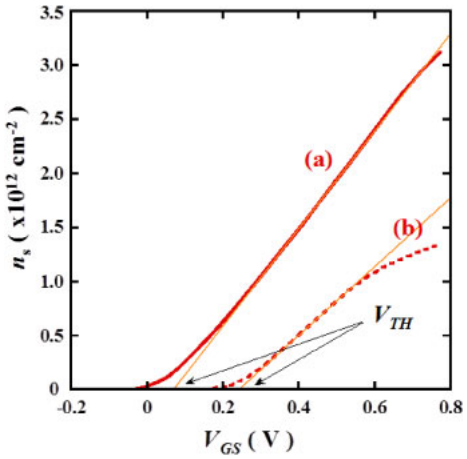

Fig. 3. (Color online) V_{GS} dependences of n_s for $Al_{0.59}In_{0.41}Sb/InSb/Al_{0.59}In_{0.41}Sb$ PHEMTs with a barrier layer thickness of 10 nm. The solid line (a) corresponds to the case of the nonparabolic energy band, and the dashed line (b) corresponds to the case of the parabolic energy band.

4. Results and discussion

First we analyzed the quantum states of InSb-PHEMTs. In Fig. 3, the dependences of n_s on V_{GS} are shown for PHEMTs. Curve (a) corresponds to the case of the nonparabolic energy band and curve (b) to the case of the parabolic energy band. The gate metal was assumed to be the same Ti/Au as used by Ashley et al.[5] Unfortunately, no available experimental data on the surface potential energy at the gate-to-source voltage V_{GS} of 0 V (i.e., the Schottky barrier height, ϕ_B between the Ti/Au metal and the $Al_{0.59}In_{0.41}Sb$ barrier layer) are reported. Therefore, it was estimated to be 0.85 eV using the following equation:[31]

$$\phi_B=\frac{2}{3}E_g. \quad (8)$$

The threshold voltage V_{TH} was estimated by extrapolating in such a way as $n_s\to 0$ in the n_s–V_{GS} curve. The value of V_{TH} was 0.07 V for case (a) and 0.24 V for case (b). A difference in V_{TH} values for the two cases is ascribed to the effect of the nonparabolicity of the conduction band for InSb.[14] In case (b), the value of n_s for InSb-PHEMTs was saturated with increasing V_{GS}, and its maximum value was $1.5\times10^{12}\,cm^{-2}$. This value is much less than that expected for InAs-PHEMTs with excellent G_m.[1] As described previously, the subband energy is well known to be inversely proportional to the effective mass m_c^* at the bottom of the conduction band, and the m_c^* of InSb is $0.0139\,m_0$.[8] Using this m_c^* value causes the subband energies of InSb-PHEMTs to be much higher than those for $In_{0.53}Ga_{0.47}As$-HEMTs and InAs-PHEMTs owing to a smaller m_c^* of electrons.

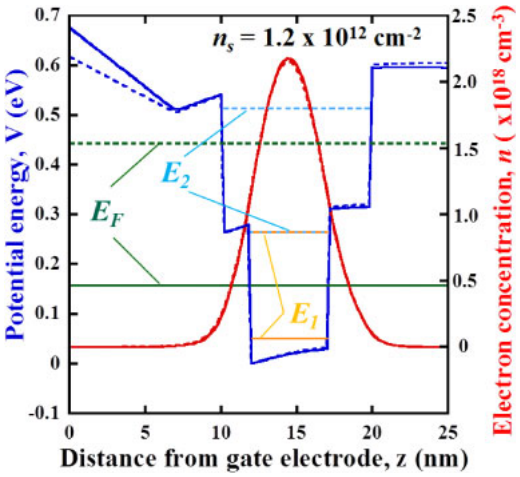

Fig. 4. (Color online) Energy states and 2DEG concentration profiles calculated for the ns of $1.2 \times 10^{12}\,\mathrm{cm}^2$ in $Al_{0.59}In_{0.41}Sb/InSb/Al_{0.59}In_{0.41}Sb$ PHEMTs with a barrier layer thickness of 10 nm. The solid lines correspond to the case of the non-parabolic band, and the dashed lines correspond to the case of the parabolic band.

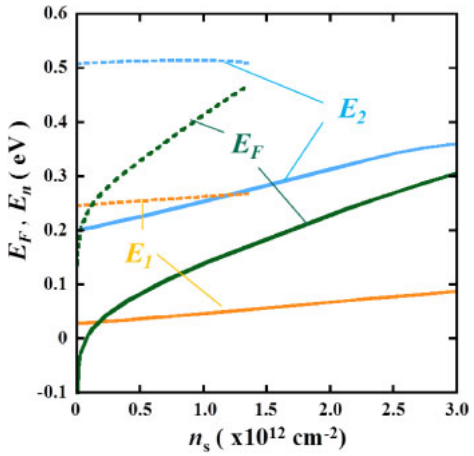

Fig. 5. (Color online) The ns dependence of En for $Al_{0.59}In_{0.41}Sb/InSb/Al_{0.59}In_{0.41}Sb$ PHEMTs with a barrier layer thickness of 10 nm. The energy was measured from the bottom of the conduction band of InSb on the upper heterojunction side. The solid lines correspond to the case of the nonparabolic band, and the dashed lines correspond to the case of the parabolic band.

As a result, the threshold voltage V_{TH} of InSb-PHEMTs shifts toward the normally-off side because E_F must be located above the subband energies to generate 2DEG in the channel. On the contrary, in case (a), the values of n_s of InSb-PHEMTs increase with increasing V_{GS} and exceed $2.5 \times 10^{12}\,\mathrm{cm}^{-2}$. The slopes in case (a) are obviously larger than those in case (b). This implies that the value of G_m calculated for the case of the parabolic energy band is smaller than that calculated for the case of the nonparabolic energy band. As seen from Eq. (1), m_c^* of InSb increases as E increases from the bottom of the conduction band because of the strong nonparabolicity of the conduction band compared with InAs and $In_{0.53}Ga_{0.47}As$. Because of this effect, the subband energies of InSb-PHEMTs are less than those estimated for the case of the parabolic energy band. Hence, a high concentration of electrons can be confined in the InSb channel layer.

Next, the energy states were calculated for the case of n_s of $1.2 \times 10^{12}\,\mathrm{cm}^{-2}$. The subband energies E_n and the concentration profiles for 2DEG are shown in Fig. 4, where the energy was measured from the bottom of the conduction band of InSb on the upper heterojunction side. The solid lines correspond to the case of the nonparabolic band and the dashed lines to the case of the parabolic band. In the case of the nonparabolic energy band, E_F and the first (E_1) and second subband (E_2) energy levels are located within the InSb well, and most of the electrons are strongly confined in the InSb layer even though its thickness is only 5 nm. This is because the effective mass of electrons increases substantially with an increase in their energy [Eq. (1)]. In the case of the parabolic energy band, although the first subband level is located near the top of the conduction-band discontinuity $\Delta E_{C,eff}$ at the $Al_{0.59}In_{0.41}Sb/InSb$ heterointerface, the second subband energy lies far above the InSb well.

The n_s dependences of E_F and E_n for InSb-PHEMTs are shown in Fig. 5, where the energy was measured from the bottom of the conduction band of InSb on the upper $Al_{0.59}In_{0.41}Sb/InSb$ heterojunction side. The solid lines correspond to the case of the nonparabolic band and the dashed lines correspond to the case of the parabolic band. In the case of the nonparabolic band, the first subband level remains within $\Delta E_{C,eff}$ at the $Al_{0.59}In_{0.41}Sb/InSb$ heterointerface over a wide range of n_s. The second subband level also remains within $\Delta E_{C,eff}$ for a relatively low ns but lies slightly above $\Delta E_{C,eff}$ for ns larger than $1.5 \times 10^{12}\,\mathrm{cm}^{-2}$. In the case of the parabolic band, on the contrary, even the first subband energy is close to $\Delta E_{C,eff}$, and the second subband energy lies far above $\Delta E_{C,eff}$.

In the case of the parabolic energy band, E_F approaches the bottom of the δ-doping layer at V_{GS} greater than 0.6 V, and then electrons begin to accumulate in the δ-doping layer (Fig. 3). At the same time, n_s of 2DEG in the channel is no longer proportional to V_{GS} and saturates with increasing V_{GS}, as shown in Fig. 3. The same phenomena have been observed in AlGaAs/GaAs HEMTs by Hirakawa et al.[32,33] For the case of the nonparabolic energy band, on the other hand, E_F is located far below the bottom of the δ-doping layer, and hence, n_s of 2DEG in the channel does not saturate, as shown in Fig. 3.

As expected, the n_s calculated for the InSb-PHEMTs is as large as that of the InAs-PHEMTs,[13] despite the $\Delta E_{C,eff}$ of the InSb-PHEMTs being two-thirds that of the InAs-PHEMTs. This is due to the strong nonparabolicity of InSb compared with InAs because the bandgap energy of InAs is about twice as large as that of InSb, and hence, the α value of InAs is about half that of InSb. In this way, it was clarified that the channel structure with the composite channel is effective in realizing not only a low mismatch strain but a high n_s, taking into account the nonparabolicity of the conduction band in the calculation of the quantum state of 2DEG in InSb-PHEMTs.

The electron effective mass may increase owing to the nonparabolicity of the conduction band. According to the results of a previous study,[14] the effective mass of electrons $\bar{m}_{c,n}^*$ in the nth subband can be obtained by averaging over the whole channel using the unperturbed wave equations:

$$\frac{1}{\bar{m}_{c,n}^*} = \int dz \frac{1}{m_c^*(z)} |\xi_n(z)|^2. \quad (9)$$

The $\bar{m}^*_{c,n}$ is calculated for the quantum state shown in Fig. 4. The $\bar{m}^*_{c,1}$ (the first subband) is 0.0161 m_0 and $\bar{m}^*_{c,2}$ (the second subband) is 0.0287 m_0, whereas the effective mass at the bottom of the conduction band m^*_c is 0.0139 m_0. Although $\bar{m}^*_{c,2}$ is twice as large as m^*_c, $\bar{m}^*_{c,1}$ is slightly larger than m^*_c. Since 95% of the electrons is found to occupy the first subband, as described in Sect. 3, the decrease in the electron mobility owing to the nonparabolicity for the conduction band is considered to be small.

5. Conclusions

We proposed an InSb-PHEMT with an InSb composite channel in which an $Al_yIn_{1-y}Sb$ sub-channel layer was inserted between the InSb channel and the $Al_xIn_{1-x}Sb$ barrier layers to increase the effective conduction-band offset ($\Delta E_{C,eff}$) between the InSb channel and the barrier layers. The channel structure of the proposed InSb-PHEMTs was decided on the basis of People's critical thickness theory. The energy states for the proposed InSb-PHEMTs were calculated by our analytical method taking account of the nonparabolicity for the conduction band. For the proposed InSb-PHEMT, putting a composite channel into the channel was found to be effective for obtaining a sufficiently large $\Delta E_{C,eff}$ (~0.563 eV) to restrain electrons in the channel. As a result, the sheet concentration (n_s) of 2DEG increased to as high as 2.5×10^{12} cm^{-2}, which is comparable to that of InAs-PHEMTs. It was confirmed that the effect of nonparabolicity on the energy states of 2DEG is greater in InSb-PHEMTs than in InAs-PHEMTs. Electrons in the proposed InSb-PHEMTs were strongly bound to the channel layer compared with those in InAs-PHEMTs, despite the effective mass at the conduction band of InSb being smaller than that of InAs and ΔE_C for InSb-PHEMTs being 25% smaller than that for InAs-PHEMTs. This is because the bandgap energy of InSb is about one-half that of InAs, and hence the nonparabolicity parameter of InSb is about twice as large as that of InAs.

1) E. Y. Chang, C. I. Kuo, H. T. Hsu, C. Y. Chiang, and Y. Miyamoto, Appl. Phys. Express **6**, 034001 (2013).
2) X. Mei, W. Yoshida, M. Lange, J. Lee, J. Zhou, P. H. Liu, K. Leong, A. Zamora, J. Padilla, S. Sarkozy, R. Lai, and W. R. Deal, IEEE Electron Device Lett. **36**, 327 (2015).
3) D. H. Kim and J. A. del Alamo, IEEE Trans. Electron Devices **57**, 1504 (2010).
4) C.-I. Kuo, H.-T. Hsu, E. Y. Chang, C.-Y. Chang, Y. Miyamoto, S. Datta, M. Radosavljevic, G.-W. Huang, and C.-T. Lee, IEEE Electron Device Lett. **29**, 290 (2008).
5) T. Ashley, M. T. Emeny, D. G. Hayes, K. P. Hilton, R. Jefferies, J. O. Maclean, S. J. Smith, A. W.-H. Tang, D. J. Wallis, and P. J. Webber, IEDM Tech. Dig., 2009, p. 849.
6) S. Datta, T. Ashley, J. Brask, L. Buckle, M. Doczy, M. Emeny, D. Hayes, K. Hilton, R. Jefferies, T. Martin, T. J. Phillips, D. Wallis, P. Wilding, and R. Chau, IEDM Tech. Dig., 2005, p. 763.
7) L. I. Schiff, *Quantum Mechanics* (McGraw-Hill, New York, 1968) p. 38.
8) C. Hermann and C. Weisbuch, Phys. Rev. B **15**, 823 (1977).
9) S. M. Sze and K. K. Ng, *Physics of Semiconductor Devices* (Wiley, New York, 2007) p. 789.
10) E. O. Kane, J. Phys. Chem. Solids **1**, 249 (1957).
11) E. O. Kane, *Semiconductors and Semimetals* (Academic Press, New York, 1966) Vol. 1, p. 75.
12) B. Mroziewicz, M. Bugajski, and W. Nakwaski, *Physics of Semiconductor Lasers* (PWN-Polish Scientific Publishers, Warsaw, 1991) p. 73.
13) Y. Nishio, S. Yamaguchi, Y. Yamazaki, A. Watanabe, T. Tange, T. Iida, and Y. Takanashi, Proc. 31st Int. Conf. Physics of Semiconductors, 2012, 37.19.
14) Y. Nishio, T. Tange, N. Hirayama, T. Iida, and Y. Takanashi, Phys. Status Solidi A **210**, 2423 (2013).
15) Y. Nishio, T. Tange, N. Hirayama, T. Iida, and Y. Takanashi, Jpn. J. Appl. Phys. **53**, 04EF09 (2014).
16) J. W. Matthews and A. E. Blakeslee, J. Cryst. Growth **27**, 118 (1974).
17) J. W. Matthews, S. Mader, and T. B. Light, J. Appl. Phys. **41**, 3800 (1970).
18) R. People and J. C. Bean, Appl. Phys. Lett. **47**, 322 (1985).
19) M. P. C. M. Krijn, Semicond. Sci. Technol. **6**, 27 (1991).
20) M. Cardona and N. E. Christensen, Phys. Rev. B **37**, 1011 (1988).
21) F. H. Pollak and M. Cardona, Phys. Rev. **172**, 816 (1968).
22) C. G. Van de Walle, Phys. Rev. B **39**, 1871 (1989).
23) A. R. Williams, J. Kubler, and C. D. Gelatt, Phys. Rev. B **19**, 6094 (1979).
24) B. Jalali, in *InP HBTs, Growth, Processing, and Applications*, ed. B. Jalali and S. J. Pearton (Artech House, Boston, MA, 1995) p. 405.
25) A. F. J. Levi and T. H. Chiu, Appl. Phys. Lett. **51**, 984 (1987).
26) A. F. J. Levi and Y. Yafet, Appl. Phys. Lett. **51**, 42 (1987).
27) D. Oertel, D. Bimberg, R. K. Bauer, and K. W. Carey, Appl. Phys. Lett. **55**, 140 (1989).
28) E. Tournié, K. H. Ploog, and C. Alibert, Appl. Phys. Lett. **61**, 2808 (1992).
29) Y. Ando and T. Itoh, IEEE Trans. Electron Devices **37**, 67 (1990).
30) H. Taguchi, H. Murakami, M. Oura, T. Iida, and Y. Takanashi, Jpn. J. Appl. Phys. **45**, 8549 (2006).
31) C. A. Mead and W. G. Spitzer, Phys. Rev. **134**, A713 (1964).
32) K. Hirakawa, H. Sakaki, and J. Yoshino, Appl. Phys. Lett. **45**, 253 (1984).
33) K. Hirakawa, H. Sakaki, and J. Yoshino, Phys. Rev. Lett. **54**, 1279 (1985).